

# A microscopic rotational cranking model and its connection to conventional cranking and other collective rotational models

P. Gulshani

NUTECH Services, 3313 Fenwick Crescent, Mississauga, Ontario, Canada L5L 5N1  
Tel. #: 647-975-8233; [matlap@bell.net](mailto:matlap@bell.net)

A simple derivation from first principles of the conventional cranking model for nuclear collective rotation about a single axis and its coupling to intrinsic motion is given. The microscopic cranking model is derived by transforming the nuclear Schrodinger equation to a rotating frame using a rotation-intrinsic product wavefunction and imposing no constraints on either the wavefunction or the nucleon coordinates. The no-constraint feature of the transformation makes it possible to share the angular momentum of the nucleus between the rotating frame and intrinsic system. The rotation of the frame is driven by a combination of rigid and irrotational flows generated by the motion of the nucleons. The resulting transformed, time-reversal invariant Schrodinger equation is readily reduced to the equations of the conventional cranking, particle-plus-rotor, phenomenological and microscopic collective rotation-vibration, and two-fluid semi-classical collective models. In particular, the reduction of the microscopic model to the conventional cranking model is described in detail with support from an application of the model to the ground-state rotational band in  $^{20}_{10}Ne$  using a self-consistent anisotropic harmonic oscillator mean-field potential. The reduction reveals some of the approximations and assumptions implied by the conventional cranking model. These revelations are also applicable to the corresponding constrained cranked Hartree-Fock model.

*PACS number:* 21.60.Ev, 21.60.Fw, 21.60.Jz

*Keywords:* canonical transformation; multi-particle rigid and irrotational flow rotation; microscopic and conventional cranking and other collective models; dynamic angular velocity; time-reversal invariance

## 1. Introduction

The self-consistent cranking model [1,2] is frequently used to study collective rotational properties of deformed nuclei [3-27 and references therein]. It has been proven to be a relatively simple, transparent, and successful method for investigating collective rotational properties and phenomena in deformed nuclei. The model assumes that the anisotropic nuclear potential  $V$  is rotating at a constant angular frequency  $\omega_{cr}$  about  $x$  or  $1$  axis. The model time-dependent Schrodinger equation:

$$i\hbar\frac{\partial}{\partial t}|\Psi_{cr}\rangle = H_{cr}|\Psi_{cr}\rangle \quad (1)$$

where:

$$H_{cr} \equiv \frac{1}{2M} \sum_{n,j=1}^{A,3} p_{nj}^2 + V_{cr}(\vec{r}_n), \quad \vec{r}_n = R(\omega_{cr} t) \vec{r}'_n \quad (2)$$

and  $R$  is an orthogonal matrix and  $\vec{r}'_n$  is the  $n^{\text{th}}$  particle coordinate relative to the rotating frame, is then unitarily transformed to the rotating frame:

$$|\Psi_{cr}\rangle = e^{-i(\omega_{cr} L + E)t/\hbar} |\Phi_{cr}\rangle \quad (3)$$

One then obtains the stationary cranking model equation<sup>1</sup>:

$$H_{cr} \cdot \bar{\Phi}_{cr} \equiv (H - \omega_{cr} \cdot L) \cdot \bar{\Phi}_{cr} = \bar{E}_{cr} \bar{\Phi}_{cr} \quad (4)$$

where  $L$  is the total angular momentum operator. The angular velocity  $\omega_{cr}$  is then determined by requiring the expectation of  $L$  to have a fixed value  $J$ :

$$\hbar J \equiv \langle \Phi_{cr} | L | \Phi_{cr} \rangle \quad (5)$$

The energy  $E_{cr}$  in a space-fixed frame is then given by:

$$E_{cr} = \langle \Phi_{cr} | H | \Phi_{cr} \rangle = \langle \Phi_{cr} | (H_{cr} + \omega_{cr} \cdot L) | \Phi_{cr} \rangle = \bar{E}_{cr} + \omega_{cr} \cdot \langle \Phi_{cr} | L | \Phi_{cr} \rangle \quad (6)$$

The physical or dynamical moment of inertia  $\mathcal{J}_d$  is then given, at each value  $J$ , by the excitation energy  $\Delta E_J$ :

$$\frac{2\mathcal{J}_d}{\hbar^2} = \frac{4J-2}{\Delta E_J - \Delta E_{J-2}} \quad (MeV)^{-1} \quad (7)$$

$$\Delta E_J \equiv E_J - E_0 \quad (8)$$

Because the rotation in the conventional cranking model is externally driven, the model is semi-classical and phenomenological in nature, and Eq. (4) is time-reversal non-invariant, and  $\omega_{cr}$  is a  $c$  number. It is therefore desirable to have a cranking model where the rotation is driven by the motions of the nucleons themselves instead of externally, i.e., it is desirable to derive the model microscopically, as suggested in [2,4,5,7, 12,18,28]. In several studies starting from first principles, Eq. (4) was derived, with various degrees of success, using canonical transformations, angular momentum projection, and generator-coordinate methods and using various

---

<sup>1</sup> Eq. (4) can also be derived from a variation of the Schrodinger equation subject to energy minimization with the wavefunction  $\Phi_{cr}$  constrained to give a fixed value for the expectation of the angular momentum.

approximations and assumptions such as redundant coordinates, large deformations, expansion in power of the angular momentum, etc. [4,5,12,18, 29-32].

In this article, we derive, simply and from first principles, a microscopic time-reversal invariant cranking type model that can be readily reduced to the conventional cranking model in Eqs. (4) and (6). The microscopic model is derived by canonically transforming the nuclear Schrodinger equation to a rotating frame that is driven by the motion of the nucleons. No constraints are imposed on either on the wavefunction or the particle coordinates. In the microscopic model, the total angular momentum is the sum of those of the rotating frame and intrinsic system. The rotation of the rotating frame is chosen to be dictated by a certain combination of rigid and irrotational flows of the nucleons.

The microscopic cranking model equation is also reduced to that of the phenomenological [33-35,3] and microscopic [36-38] nuclear collective rotation-vibration models. It is also reduced to the equation of the phenomenological nuclear particle-plus-rotor model [4-7,8,12,28,39] and other microscopic and phenomenological collective models [40-45].

In Section 2, we present the derivation of the microscopic cranking-model Schrodinger equation. In Section 3, we solve the microscopic cranking-model Schrodinger equation using a self-consistent single-particle mean-field anisotropic harmonic oscillator potential. In Section 4 we use the model to predict the excitation energy and quadrupole moment in the ground-state rotational band of the nucleus  $^{20}_{10}Ne$  and compare the results with those of the conventional cranking model and with empirical data. In Section 5, we reduce the microscopic cranking model equation to that of the conventional cranking model assuming small rotating-frame angular momentum and an appropriate microscopic prescription for the combination of the rigid and irrotational flows. In Section 5, we also reduce the microscopic cranking model equation to the equation of each of the models mentioned in the preceding paragraph. Section 6 presents concluding remarks.

## 2. Derivation of microscopic rigid-irrotational flow cranking model

The microscopic cranking model is derived by transforming the nuclear Schrodinger equation (instead of the Hamiltonian) to a reference frame rotating about the  $x$  or 1 axis, defined by the collective angle  $\theta(x_{nj})$ , and using the product wavefunction (similar to that in [46])<sup>2</sup>:

$$\Psi = G(\theta) \cdot \Phi(x_{nj}) \quad (9)$$

where  $x_{nj}$  ( $n = 1, \dots, A$ ;  $j = 1, 2, 3$ , where  $A$  = nuclear mass number) are the space-fixed nucleon coordinates. The angle  $\theta$  defines the orientation in space of the anisotropic particle distribution (such as quadrupole distribution) described by the intrinsic wavefunction  $\Phi$ , which is assumed

---

<sup>2</sup> The wavefunction in Eq. (9) is a one-dimensional version of the nuclear-rotor-model wavefunction [4,6,7,12].

to be a function of the space-fixed particle coordinates. Applying  $\frac{\partial}{\partial x_{nj}}$  and  $\frac{\partial^2}{\partial x_{nj}^2}$  to  $\Psi$  in Eq. (9), we obtain:

$$\frac{\partial \Psi}{\partial x_{nj}} = \frac{\partial G}{\partial x_{nj}} \Phi + G \frac{\partial \Phi}{\partial x_{nj}} \quad (10)$$

$$\begin{aligned} \frac{\partial^2 \Psi}{\partial x_{nj}^2} &= \frac{\partial^2 G}{\partial x_{nj}^2} \Phi + 2 \frac{\partial G}{\partial x_{nj}} \cdot \frac{\partial \Phi}{\partial x_{nj}} + G \frac{\partial^2 \Phi}{\partial x_{nj}^2} \\ &= \Phi \frac{\partial \theta}{\partial x_{nj}} \cdot \frac{\partial}{\partial \theta} \left( \frac{\partial \theta}{\partial x_{nj}} \cdot \frac{\partial G}{\partial \theta} \right) + 2 \frac{\partial \theta}{\partial x_{nj}} \cdot \frac{\partial G}{\partial \theta} \cdot \frac{\partial \Phi}{\partial x_{nj}} + G \frac{\partial^2 \Phi}{\partial x_{nj}^2} \end{aligned} \quad (11)$$

Substituting Eq. (11) into the Schrodinger equation:

$$H \cdot \Psi \equiv \left( \frac{1}{2M} \sum_{n,j=1}^{A,3} p_{nj}^2 + V \right) \cdot \Psi = E \cdot \Psi \quad (12)$$

where  $M$  is the nucleon mass, we obtain:

$$G \cdot H \cdot \Phi - \frac{\hbar^2}{M} \cdot \sum_{n,j} \frac{\partial \theta}{\partial x_{nj}} \cdot \frac{\partial G}{\partial \theta} \cdot \frac{\partial \Phi}{\partial x_{nj}} - \frac{\hbar^2}{2M} \cdot \Phi \cdot \sum_{n,j} \frac{\partial \theta}{\partial x_{nj}} \cdot \frac{\partial}{\partial \theta} \left( \frac{\partial \theta}{\partial x_{nj}} \cdot \frac{\partial G}{\partial \theta} \right) = E \cdot \Phi \quad (13)$$

We require the rotation of the frame through the angle  $\theta$  to be generated by the motion of the particles and hence by the angular momentum operator  $L$  along  $x$  or 1. Therefore,  $\theta$  and  $L$  are a canonically conjugate pair, satisfying the commutation relation:

$$[\theta, L] = i\hbar \Rightarrow L \equiv \sum_n (y_n p_{nz} - z_n p_{ny}) = -i\hbar \frac{\partial}{\partial \theta} \quad (14)$$

Substituting Eq. (14) into Eq. (13), we obtain:

$$G \cdot H \cdot \Phi + \frac{1}{M} \cdot \sum_{n,j} \frac{\partial \theta}{\partial x_{nj}} \cdot (L \cdot G) \cdot p_{nj} \cdot \Phi + \frac{1}{2M} \cdot \Phi \cdot \sum_{n,j} \frac{\partial \theta}{\partial x_{nj}} \cdot L \cdot \left( \frac{\partial \theta}{\partial x_{nj}} \cdot L \cdot G \right) = E \cdot \Phi \quad (15)$$

Next we assume that  $G$  is an eigenstate of  $L$ :

$$L e^{il\theta} = \hbar \gamma e^{i\gamma\theta} \quad (16)$$

where  $\hbar \gamma$  is the angular momentum associated with the rotating frame.  $\gamma$  is determined in Sections 2.1 and 2.2 and Section 5. Substituting Eq. (16) into Eq. (15), we obtain:

$$\begin{aligned}
H \cdot \boldsymbol{\Phi} + \frac{\hbar\gamma}{M} \cdot \sum_{n,j} \frac{\partial \theta}{\partial x_{nj}} \cdot p_{nj} \cdot \boldsymbol{\Phi} + \frac{\hbar^2\gamma^2}{2M} \cdot \sum_{n,j} \frac{\partial \theta}{\partial x_{nj}} \cdot \frac{\partial \theta}{\partial x_{nj}} \cdot \boldsymbol{\Phi} \\
+ \frac{\hbar\gamma}{4M} \cdot \boldsymbol{\Phi} \cdot \sum_{n,j} \cdot L \cdot \left( \frac{\partial \theta}{\partial x_{nj}} \cdot \frac{\partial \theta}{\partial x_{nj}} \right) = E \cdot \boldsymbol{\Phi}
\end{aligned} \tag{17}$$

We now choose  $\theta$  to satisfy the relation (for rotation about  $x$  or 1 axis only)<sup>3</sup>:

$$\frac{\partial \theta}{\partial x_{nj}} = \sum_{k=1}^2 \chi_{jk} x_{nk}, \quad \chi_{jk} = 0 \text{ for } j, k \neq 2, 3 \tag{18}$$

The real 3x3 matrix  $\chi$  can be chosen to be a sum of different types of matrices, each describing different types of physical motion such as quadrupole rigid and irrotational, and non-quadrupole rigid flow regimes described in [40-45,47-49]. In this article, we choose  $\chi$  to be the sum of a symmetric and an antisymmetric matrices so that the non-zero elements of  $\chi$  are  $\chi_{23} \equiv \chi_2 + \chi_3$ , and  $\chi_{32} = -\chi_2 + \chi_3$ . We choose  $\chi_3 = \lambda \cdot \chi_2$  and hence:

$$\chi_{23} \equiv (1 + \lambda) \cdot \chi_2, \quad \text{and} \quad \chi_{32} = -(1 - \lambda) \cdot \chi_2 \tag{19}$$

Substituting Eq. (19) into  $[\theta, L] = i\hbar$  in Eq. (14), we obtain:

$$\chi_2 = -(\mathcal{J}_+ - \lambda \cdot \mathcal{J}_-)^{-1} \equiv -\mathcal{J}^{-1} \tag{20}$$

where:

$$\mathcal{J}_+ \equiv \sum_n (y_n^2 + z_n^2), \quad \mathcal{J}_- \equiv \sum_n (y_n^2 - z_n^2) \tag{21}$$

Substituting Eqs. (18)-(20) into Eq. (17), we obtain:

---

<sup>3</sup> Classically,  $\frac{\partial \theta}{\partial x_{nj}}$  may be considered to be the collective component of the particle velocity field, refer to [46] for more detail.

more detail. For any linear (in Eq. (18)) or other flow prescription for  $\theta$ , one can prove (using Eqs. (18)-(20) or Stoke's theorem, refer to [46, Eq. (57)]) that, for a system of more than one particle, the mixed second partial derivatives of  $\theta$  are discontinuous, i.e.,  $\vec{\nabla}_n \times \vec{\nabla}_n \theta \neq 0$ . This discontinuity seems to be related to the observation that a change  $\delta\theta$  in the collective angle  $\theta$  corresponds to different sets of changes  $\delta\vec{r}_n$  in the particle positions in a multi-particle system. Even for a single particle,  $\vec{\nabla} \times \vec{\nabla} \theta \neq 0$  at the coordinate system origin. However, this discontinuity is of no consequence for the analysis presented in this article because no mixed second derivative of  $\theta$  appears anywhere in the analysis and all the derived variables are continuous and well behaved.

$$\left[ H + \frac{\hbar\gamma}{M\mathcal{J}} \cdot (L - \lambda \cdot T) + \frac{\hbar^2\gamma^2}{2M\mathcal{J}^2} \cdot \left[ (1 + \lambda^2) \cdot \mathcal{J}_+ - 2\lambda \cdot \mathcal{J}_- \right] + \frac{2i\hbar^2\gamma\lambda^2}{M\mathcal{J}^3} \cdot (\lambda \cdot \mathcal{J}_+ - \mathcal{J}_-) \cdot \sum_n y_n z_n \right] \cdot \boldsymbol{\Phi} = E \cdot \boldsymbol{\Phi} \quad (22)$$

where  $T$  is a linear shear operator, generating a linear irrotational flow, and defined by:

$$T \equiv \sum_n (y_n p_{nz} + z_n p_{ny}) \quad (23)$$

The first term on the left-hand-side of Eq. (22) is the intrinsic energy of the interacting nucleons. The second term on the left-hand-side of Eq. (22) is the cranking or Coriolis energy term, i.e., the energy associated with the interaction of the motion of the nucleons with the rotating frame. The third term on the left-hand-side of Eq. (22) is the kinetic energy of the collective rotation of the nucleus as a whole with the rotating frame. It may be viewed as a centrifugal energy. The remaining term on the left-hand-side of Eq. (22) arises from the interaction of the collective rotation with fluctuation/vibrations in the rotating-frame angular velocity (defined in Sections 2.1 and 2.2) and intrinsic moments of inertia appearing in Eqs. (20) and (21). These remarks and those in [39] may provide a better understanding of the various interactions involved in the rotational motion.

## 2.1 Rigid-flow rotating frame

For  $\lambda = 0$  (i.e., for the rigid flow rotating frame), Eq. (22) reduces to:

$$\left( H + \frac{\hbar\gamma}{M\mathcal{J}_+} \cdot L + \frac{\hbar^2\gamma^2}{2M\mathcal{J}_+} \right) \cdot \boldsymbol{\Phi} = E \cdot \boldsymbol{\Phi} \quad (24)$$

where  $M\mathcal{J}_+$  is the rigid-flow moment of inertia (defined in Eq. (21)) and commutes with  $L$ . Expressed in terms of the rigid-flow angular frequency  $\omega_{rig}$  of the rotating frame:

$$\omega_{rig} \equiv \frac{\hbar\gamma}{M\mathcal{J}_+}, \quad (25)$$

Eq. (24) becomes:

$$\left( H + \omega_{rig} \cdot L + \frac{1}{2} \omega_{rig}^2 \cdot M\mathcal{J}_+ \right) \cdot \boldsymbol{\Phi} = E \cdot \boldsymbol{\Phi} \quad (26)$$

Eq. (26) resembles the conventional cranking model equation in a space-fixed frame given in Eq. (6), but differs from Eq. (6) by the rigid-flow centrifugal energy term (third term on the left-hand-side of Eq. (26)), and by the microscopically defined  $\omega_{rig}$  instead of the constant

parameter  $\omega_{cr}$  in Eq. (6). Eq. (26) also differs from the cranking model Eq. (4) in the rotating frame by the aforementioned terms and by the sign of  $\omega_{rig}$  term (note that the microscopic cranking model solves Eq. (26) whereas the conventional cranking model solves Eq. (4) and not Eq. (6)). Eq. (26) is time-reversal invariant whereas Eq. (6) is not.

We determine the rotating frame angular momentum  $\hbar\gamma$  in Eq. (25) by requiring the expectation of the total angular momentum operator  $L$  with respect to the wavefunction  $\Psi$  in Eq. (9) to have the empirically observed rotational-band excited-state angular momentum  $\hbar J$ <sup>4</sup>:

$$\hbar J = \langle \Psi | L | \Psi \rangle = \langle G | L | G \rangle + \langle \Phi | L | \Phi \rangle = \hbar\gamma + \hbar l = \omega_{rig} \cdot M \cdot \mathcal{J}_+ + \hbar l \quad (27)$$

where:

$$\hbar l \equiv \langle \Phi | L | \Phi \rangle \quad (28)$$

The prescription in Eq. (27) is a generalization of the conventional cranking model Eq. (5) and reduces to it for small the angular momentum  $\hbar\gamma$  of the rotating frame.

It follows from Eq. (27) that, in the microscopic cranking model,  $\gamma$  (and hence  $\omega_{rig}$ ) and  $l$  can have different signs, and hence the rotating frame and the intrinsic system may rotate in opposite directions, unlike that in the conventional cranking model but similarly to that in the phenomenological nuclear particle-plus-rotor model [4-7,12,28,39].

The excitation energy and physical or dynamic moment of inertia are defined in Eqs. (7) and (8). The rigid-flow moment of inertia  $\mathcal{J}_+$  in Eqs. (24)-(26) may be called the kinematic moment of inertia.

The above-stated differences between the microscopic and conventional cranking models generate some significant differences in the predictions of the two models as is demonstrated in Section 4.

## 2.2 Rigid-plus-irrotational flow rotating frame

For  $\lambda \neq 0$  (i.e., for a frame rotation governed by combined rigid and irrotational flows), Eq. (22) generalizes the microscopic cranking model Eq. (24) or (26) to include linear shear flow kinematics and allows a closer connection with the conventional cranking model as shown in Section 5. We express Eq. (22) in the following cranking-model form:

---

<sup>4</sup> The value of  $\gamma$  determined by Eq. (27) may be viewed as an approximation (implied by the conventional cranking model) to an integer value of  $\gamma$  needed to ensure that  $\Psi$  in Eq. (9) is a single-valued function of  $\theta$ .

$$\left\{ H + \omega_{rs} \cdot (L - \lambda \cdot T) + \frac{M\omega_{rs}^2}{2} \cdot \left[ (1 + \lambda^2) \cdot \mathcal{J}_+ - 2\lambda \cdot \mathcal{J}_- \right] + \frac{2i\hbar\omega_{rs}\lambda^2}{M\cdot\mathcal{J}^2} \cdot (\lambda \cdot \mathcal{J}_+ - \mathcal{J}_-) \cdot \sum_n y_n z_n \right\} \cdot \Phi = E \cdot \Phi \quad (29)$$

where the rigid-plus-shear-flow angular frequency  $\omega_{rs}$  of the rotating frame is defined by:

$$\omega_{rs} \equiv \frac{\hbar\gamma}{M \cdot \mathcal{J}}, \quad (30)$$

The order of the appearance of the operators in the second term on the left-hand-side in Eq. (29) is immaterial because we can readily show that:

$$[\mathcal{J}, L - \lambda \cdot T] = 0 \quad (31)$$

for any c-number  $\lambda$ .

The excitation energy and physical or dynamic moment of inertia are defined in Eqs. (7) and (8). The variable  $\mathcal{J}$  in Eq. (30) may be called the kinematic moment of inertia associated with the Coriolis energy term, i.e. the inertial mass associated with the interaction of the motion of the nucleons with the rotating frame. This inertia differs from the kinematic moment of inertia  $[(1 + \lambda^2) \cdot \mathcal{J}_+ - 2\lambda \cdot \mathcal{J}_-] = 2\mathcal{J} - (1 - \lambda^2) \cdot \mathcal{J}_+$  in Eq. (29) that is associated with the kinetic energy of the collective rotation of the nucleus as a whole with the rotating frame, i.e., with the centrifugal energy. The Coriolis energy term modifies the intrinsic system properties such as its natural frequencies. On the other hand, the centrifugal energy term contributes more to the collective-rotation excitation energy than does the Coriolis energy term. In contrast, in the conventional cranking model (Eq. (6)), the Coriolis energy term affects both the intrinsic system properties and excitation energy.

We determine the rotating-frame angular momentum  $\hbar\gamma$  in Eq. (30) by requiring the expectation of the total angular momentum operator  $L$  with respect to the wavefunction  $\Psi$  in Eq. (9) to have the experimentally observed rotational-band excited-state angular momentum  $\hbar J$ <sup>5</sup>:

$$\hbar J = \langle \Psi | L | \Psi \rangle = \langle G | L | G \rangle + \langle \Phi | L | \Phi \rangle = \hbar\gamma + \hbar l = \omega_{rs} \cdot M \cdot \mathcal{J} + \hbar l \quad (32)$$

where:

---

<sup>5</sup> The value of  $\gamma$  determined by Eq. (32) may be viewed as an approximation (implied by the conventional cranking model) to an integer value of  $\gamma$  needed to ensure that  $\Psi$  is single-valued function of  $\theta$ .

$$\hbar l \equiv \langle \Phi | L | \Phi \rangle \quad (33)$$

The prescription in Eq. (32) differs from that in Eq. (5) for the conventional cranking model by the angular momentum  $\hbar\gamma$  of the rotating frame, and reduces to it for small  $\hbar\gamma$ .

It follows from Eq. (32) that, in the microscopic cranking model,  $\gamma$  (and hence  $\omega_{rs}$ ) and  $l$  can have different signs, and hence the rotating frame and intrinsic system may rotate in opposite directions, unlike that in the conventional cranking model.

The above-stated differences between the microscopic and conventional models generate some significant differences in the predictions of the two models as is demonstrated in Section 4.

### 3. Solutions of Eqs. (4), (26), and (29)

In this section, we determine the solutions of Eqs. (4), (26), and (29) for a mean-field anisotropic harmonic oscillator Hamiltonian:

$$H = \frac{1}{2M} \cdot \sum_{n,j=1}^{A,3} p_{nj}^2 + \frac{M\omega_1^2}{2} \cdot \sum_n x_n^2 + \frac{M\omega_2^2}{2} \cdot \sum_n y_n^2 + \frac{M\omega_3^2}{2} \cdot \sum_n z_n^2 \quad (34)$$

#### 3.1 Solution of conventional cranking model Eq. (4)

The solution to Eq. (4) has been obtained by a number of investigators [50-54] using a canonical or unitary transformation to eliminate the cross terms  $y_n p_{nz}$  and  $z_n p_{ny}$  in Eq. (4), and thereby obtain the following transformed harmonic oscillator Hamiltonian:

$$\bar{H}_{cr} = \frac{1}{2M} \cdot \sum_{n,j=1}^{A,3} p_{nj}^2 + \frac{M\omega_1^2}{2} \cdot \sum_n x_n^2 + \frac{M\alpha_2^2}{2} \cdot \sum_n y_n^2 + \frac{M\alpha_3^2}{2} \cdot \sum_n z_n^2 \quad (35)$$

and the energy eigenvalue in the rotating frame:

$$\bar{E}_{cr} = \hbar\omega_1\Sigma_1 + \hbar\alpha_2\Sigma_2 + \hbar\alpha_3\Sigma_3 \quad (36)$$

and the energy in a space-fixed frame (from Eq. (6)):

$$E_{cr} = \bar{E}_{cr} + \omega_{cr} \cdot \langle \Phi_{cr} | L | \Phi_{cr} \rangle \quad (37)$$

where:

$$\alpha_2^2 \equiv \omega_+^2 + \omega_{cr}^2 + \sqrt{\omega_-^4 + 8\omega_{cr}^2\omega_+^2}, \quad \alpha_3^2 \equiv \omega_+^2 + \omega_{cr}^2 - \sqrt{\omega_-^4 + 8\omega_{cr}^2\omega_+^2} \quad (38)$$

$$\omega_+^2 \equiv \frac{\omega_2^2 + \omega_3^2}{2}, \quad \omega_-^2 \equiv \frac{\omega_2^2 - \omega_3^2}{2}, \quad \Sigma_k \equiv \sum_{n_k=0}^{n_{kf}} (n_k + 1/2) \quad (39)$$

where  $n_{kf}$  is the number of oscillator quanta in the  $k^{\text{th}}$  direction at the Fermi surface.

For  $\bar{H}_{cr}$  in Eq. (35) to approximate a Hartree-Fock mean-field Hamiltonian, the energy  $\bar{E}_{cr}$  in Eq. (36) is minimized with respect to the frequencies  $\omega_k$  ( $k = 1, 2, 3$ ) at a fixed value of  $J$  and hence of  $\omega_{cr}$  given by the constraint in Eq. (5), and subject to the constant nuclear-quadrupole-volume condition:

$$\langle x^2 \rangle \cdot \langle y^2 \rangle \cdot \langle z^2 \rangle = c_o \quad (40)$$

where  $\langle x_k^2 \rangle \equiv \langle \bar{\Phi}_{cr} | \sum_n x_{nk}^2 | \bar{\Phi}_{cr} \rangle$  ( $k = 1, 2, 3$ ) and  $c_o$  is a constant. This minimization yields a self-consistency between the shapes of nuclear equi-potential and equi-density surfaces [7,50-53]. The minimization is performed numerically [52,53].

### 3.2 Solution of microscopic cranking model Eqs. (26) and (29)

The variable  $\mathcal{J}^{-1}$  in Eqs. (29) and (30) is a many-body operator. To find a solution of Eq. (29), we may regard  $\mathcal{J}$  as an independent dynamical collective variable and transform Eq. (29) to  $\mathcal{J}$  using the method suggested in [38,55,56]. This approach would account for the interaction of fluctuations in  $\mathcal{J}$  with the rotation. However, in this article, we are interested in collective rotational motion in absence of fluctuations in  $\mathcal{J}$  and hence in  $\omega_{rs}$ ,  $\mathcal{J}_+$ ,  $\mathcal{J}_-$ , and other similar variables in Eq. (29) and (30) because we are interested in comparing the model with the conventional cranking model, which ignores such fluctuations. Furthermore, a preliminary calculation seems to indicate that the fluctuations have a relatively small effect on the rotational motion. Therefore, in this article, we replace these variables by their expectation values in the state  $\Phi$  (thereby suppressing the fluctuations in  $\mathcal{J}$  and hence in  $\omega_{rs}$ ,  $\mathcal{J}_+$  and  $\mathcal{J}_-$  in Eqs. (29) and (30) and their interaction with the collective rotation), as follows:

$$\mathcal{J}^o \equiv \langle \Phi | \mathcal{J} | \Phi \rangle = \langle \Phi | \mathcal{J}_+ | \Phi \rangle - \lambda \langle \Phi | \mathcal{J}_- | \Phi \rangle \equiv \mathcal{J}_+^o - \lambda \mathcal{J}_-^o \quad (41)$$

$$\omega_{rs}^o \equiv \frac{\hbar\gamma}{M\mathcal{J}^o}, \quad (42)$$

Eq. (29) then becomes (note that the expectation value of  $\sum_n y_n z_n$  in Eq. (29) vanishes):

$$\left\{ H + \omega_{rs}^o \cdot (L - \lambda \cdot T) + \frac{1}{2} \omega_{rs}^{o2} M \cdot \left[ (1 + \lambda^2) \cdot \mathcal{J}_+^o - 2\lambda \cdot \mathcal{J}_-^o \right] \right\} \cdot \Phi = E \cdot \Phi \quad (43)$$

The solution of Eq. (43) is obtained similarly to that of Eq. (4) in Section 3.1 (and specialized to the solution of Eq. (26) by setting  $\lambda$  to zero). We then obtain the transformed harmonic oscillator Hamiltonian:

$$\bar{H} = \frac{1}{2M} \cdot \sum_{n,j=1}^{A,3} p_{nj}^2 + \frac{M\omega_1^2}{2} \cdot \sum_n x_n^2 + \frac{M\alpha_2^2}{2} \cdot \sum_n y_n^2 + \frac{M\alpha_3^2}{2} \cdot \sum_n z_n^2 \quad (44)$$

and the energy eigenvalue in the rotating frame:

$$\bar{E} \equiv E - \frac{1}{2} \omega_{rs}^{o,2} \cdot M \cdot \left[ (1 + \lambda^2) \cdot \mathcal{J}_+^o - 2\lambda \cdot \mathcal{J}_-^o \right] = \hbar\omega_1\Sigma_1 + \hbar\alpha_2\Sigma_2 + \hbar\alpha_3\Sigma_3 \quad (45)$$

where:

$$\alpha_2^2 \equiv \omega_+^2 + (1 - \lambda^2) \cdot \omega_{rs}^{o,2} + \sqrt{\omega_-^4 + 8\omega_{rs}^{o,2} \cdot \omega_\lambda^2}, \quad \alpha_3^2 \equiv \omega_+^2 + (1 - \lambda^2) \cdot \omega_{rs}^{o,2} - \sqrt{\omega_-^4 + 8\omega_{rs}^{o,2} \cdot \omega_\lambda^2} \quad (46)$$

where  $\Sigma_k$  is defined in Eq. (39), and:

$$\omega_\lambda^2 \equiv \omega_+^2 + \lambda \cdot \omega_-^2 \quad (47)$$

The energy in the space-fixed frame is then given by:

$$E = \frac{1}{2} \omega_{rs}^{o,2} \cdot M \cdot \left[ (1 + \lambda^2) \cdot \mathcal{J}_+^o - 2\lambda \cdot \mathcal{J}_-^o \right] + \hbar\omega_1\Sigma_1 + \hbar\alpha_2\Sigma_2 + \hbar\alpha_3\Sigma_3 \quad (48)$$

For  $\bar{H}$  in Eq. (44) to approximate a Hartree-Fock mean-field Hamiltonian, we minimize the energy  $E$  in Eq. (48) with respect to the frequencies  $\omega_k$  ( $k = 1, 2, 3$ ) at a fixed value of  $J$  and hence of  $\mathcal{J}^o$ ,  $\omega_{rs}^o$ ,  $\mathcal{J}_+^o$ , and  $\mathcal{J}_-^o$  given by the constraint in Eq. (32), and subject to the constant nuclear-quadrupole-volume condition:

$$\langle x^2 \rangle \cdot \langle y^2 \rangle \cdot \langle z^2 \rangle = c_o \quad (49)$$

where  $\langle x_k^2 \rangle \equiv \langle \Phi | \sum_n x_{nk}^2 | \Phi \rangle$  ( $k = 1, 2, 3$ ) and  $c_o$  is a constant. This minimization yields a self-consistency between the shapes of nuclear equi-potential and equi-density surfaces [7,50-53]. The minimization is performed numerically as in [52,53].

We may determine the arbitrary parameter  $\lambda$  in Eq. (48) by minimizing the energy  $E$  in Eq. (48) with respect to  $\lambda$ . A study of the results of the above derivations and the calculation in Section 4 shows that most terms in  $\lambda$  in the derived expressions cancel one another and the remaining terms in  $\lambda$  are negligibly small. Therefore, the contribution to the energy  $E$  in Eq. (48) from the operator  $\lambda \cdot T$  in Eq. (43) is small and the term  $\lambda \cdot T$  in Eq. (43) can be ignored. Therefore, the minimization of the energy  $E$  in Eq. (48) with respect to  $\lambda$  yields:

$$\lambda = \frac{\mathcal{J}_-^o}{\mathcal{J}_+^o} \quad (50)$$

Substituting Eq. (50) into Eq. (48), we obtain:

$$E = \frac{\omega_{rs}^o \cdot M}{2\mathcal{J}_+^o} \cdot [\mathcal{J}_+^{o2} - \mathcal{J}_-^{o2}] + \hbar\omega_1\Sigma_1 + \hbar\alpha_2\Sigma_2 + \hbar\alpha_3\Sigma_3 \quad (51)$$

Now  $\mathcal{J}_-$  decreases with  $J$  and vanishes at some  $J$  depending on parameters  $\omega_{rs}^o$  and  $\alpha_k$ . When this happens, the first term on the right-hand-side of Eq. (51) reduces to the rigid-flow centrifugal kinetic energy.

#### 4. Model predictions for $^{20}_{10}Ne$

In this section we present the results of the application of the microscopic cranking model described in Sections 2.1, 2.2 and 3.2 to the nucleus  $^{20}_{10}Ne$  and compare these results with those of the conventional cranking model in Sections 1 and 3.1 and with the measured data.

For  $^{20}_{10}Ne$ , we use the anisotropic-harmonic-oscillator nucleon-occupation configuration  $(\Sigma_1, \Sigma_2, \Sigma_3) = (14, 14, 22)$ , with the spherical harmonic oscillator frequency  $\hbar\omega_o = 35.4 \cdot A^{-1/3} MeV$  as in [52,53].

##### 4.1 Rigid-flow rotating frame

For the rigid-flow rotating-frame case described in Section 2.1 (i.e. for  $\lambda = 0$ ), we have performed model calculations for  $^{20}_{10}Ne$  using various versions of the self-consistency conditions to learn how the model behaves. The results of this survey are presented and possible physical explanations are given.

Fig 1 compares the excitation energy  $\Delta E_J$  measured and predicted by the microscopic and conventional cranking models when the  $\omega_k$ 's are kept constant at their ground-state (i.e.,  $J = 0$ ) self-consistent values (i.e., the nucleus remains prolate at all  $J$  values). Fig 1 shows that the microscopic cranking model predicts well the excitation energy and the conventional cranking model predicts a slightly lower  $\Delta E_J$ . The measured and predicted excitation energies increase with  $J$ , except at  $J = 8$  where the measured  $\Delta E_J$  is significantly lower than that predicted by either of the models. This difference may be attributed to a Coriolis-force induced partial alignment with the rotation axis of the quasi-particle angular momenta, which effect is not included in the models. We note that the rotational band predicted by either the microscopic or conventional cranking model does not terminate at  $J = 8$  as expected because no nuclear shape transition occurs for the particular self-consistency used.

Fig 2 shows that the measured quadrupole moment  $Q_o$  decreases monotonically with  $J$  and there is a sharp drop in  $Q_o$  at  $J = 8$  when the nucleus presumably becomes symmetric about the rotation axis (i.e., when  $\omega_2$  and  $\omega_3$  become equal). The microscopic and conventional cranking models predict lower  $Q_o$ , which decreases gradually up to  $J = 4$  in the microscopic model and up

to  $J = 8$  in the conventional cranking model, and increases above these  $J$  values (the increase in  $Q_o$  for the cranking model is not included in Fig 2).

The intrinsic angular momentum predicted by the microscopic model decreases from about  $-6.5\hbar$  at  $J = 2$  to  $-8\hbar$  at  $J = 8$ , and in this range of  $J$ , the angular momentum of the rotating frame increases from  $8.5\hbar$  to  $16\hbar$ . The predicted rotational band terminates above  $J = 23$  when the intrinsic oscillator frequency  $\alpha_3$  vanishes and hence the model governing equations have no solutions. The results in Fig 2 indicate that, to predict the observed change in the shape of the nucleus (i.e.,  $Q_o$ ) the microscopic and conventional cranking models must account for nuclear volume conservation at all  $J$  values as is normally done.

Figs 3 and 4 show respectively the excitation energies and quadrupole moment when we use the  $\omega_k$  values determined self-consistently at all  $J$  values. The conventional cranking model predicts higher  $\Delta E_J$  above  $J = 4$ , and a  $Q_o$  that decreases similarly to the observed  $Q_o$  up to  $J = 6$ , above which point the nucleus becomes progressively axially symmetric about the rotation axis (i.e.,  $\omega_2$  and  $\omega_3$  become equal) and the rotational band terminates at  $J = 8$ . The microscopic model predicts significantly higher  $\Delta E_J$ , and a  $Q_o$  that decreases rapidly up to  $J = 4$  and increases slightly thereafter. The predicted intrinsic angular momentum decreases from  $-6.5\hbar$  at  $J = 2$  to  $-8\hbar$  at  $J \geq 4$ , and the rotating-frame angular momentum is  $8.5\hbar$  at  $J = 2$  and  $12\hbar, 14\hbar, 16\hbar$  at  $J = 4, 6, 8$  respectively.

The results presented above show that the microscopic cranking model with the rigid flow rotating frame predicts somewhat similar results to those of the conventional cranking model. However, the rotations of the intrinsic system and rotating frame are in opposite directions, and the intrinsic system angular momentum reaches its limiting value of  $-8\hbar$  at  $J = 2$  and remains at this value thereafter while the rotating-frame angular momentum continues to increase with  $J$ , unlike the situation in the conventional cranking model, where the intrinsic angular momentum is equal to  $J$  at all values of the rotating-frame angular velocity.

## 4.2 Rigid-plus-irrotational flow rotating frame

For the rigid-plus-linear irrotational flow case described in Section 2.2 (i.e. for  $\lambda \neq 0$ ), Fig 5 shows the excitation energy predicted by Eq. (51) (i.e., for the value of  $\lambda$  given in Eq. (50)). The predicted excitation energy is significantly higher than that measured. However, at  $J = 2$ , the predicted excitation energy ( $6.76\text{ MeV}$ ) for  $\lambda \neq 0$  is lower than ( $8.19\text{ MeV}$ ) for the rigid-flow case (i.e., for  $\lambda = 0$ ) in Fig 3. This result indicates that the addition of the irrotational flow component in Eq. (18) reduces the excitation energy. This reduction is not sufficiently large particularly at higher  $J$  values because  $\mathcal{J}_o$  in Eq. (50) is small at  $J = 2$  and vanishes above  $J = 2$ . One reason for low value of  $\mathcal{J}_o$  is the large value of  $\omega_{rs}^o$  predicted by the constraint in Eq. (32).

The discrepancy between the microscopic and conventional cranking models mentioned in the preceding paragraph is resolved in Section 5 where we examine conditions needed to reduce the value of  $\omega_{rs}^o$  and increase the value of  $\mathcal{J}^o$ , and thereby reduce the microscopic cranking model Eq. (48) to the conventional cranking model Eq. (6).

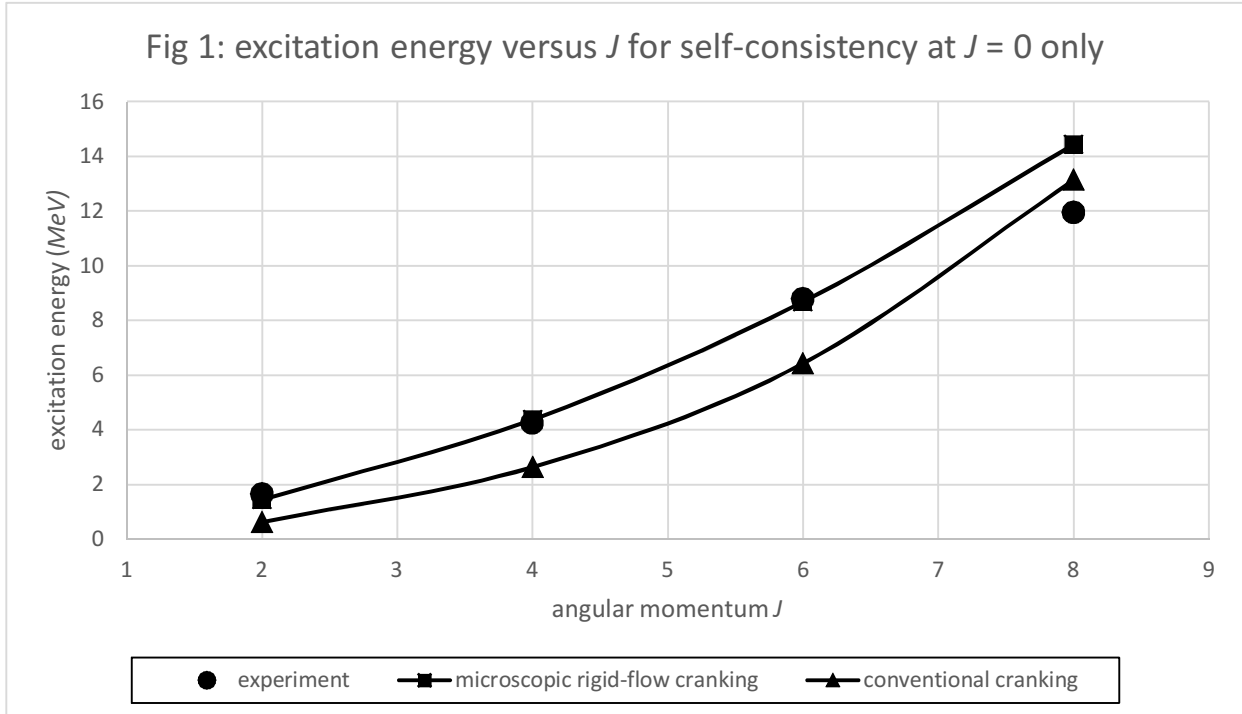


Fig 2: quadrupole moment versus  $J$  for self-consistency at  $J = 0$  only

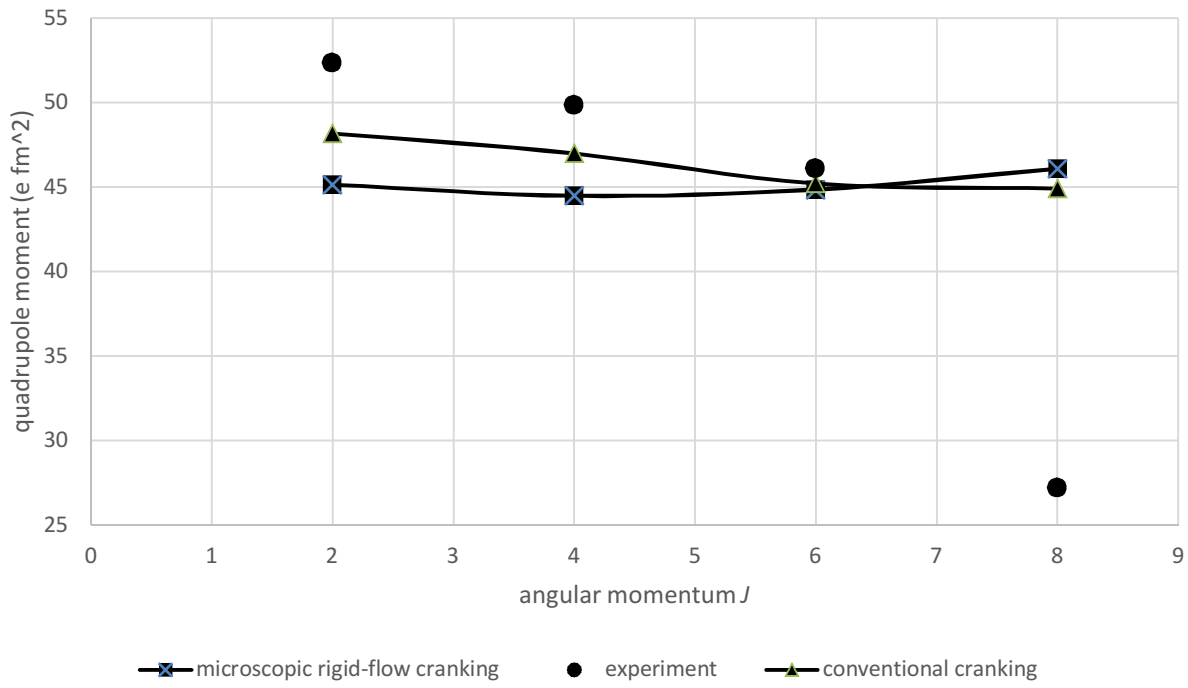


Fig 3: excitation energy versus  $J$  for self-consistency at all  $J$

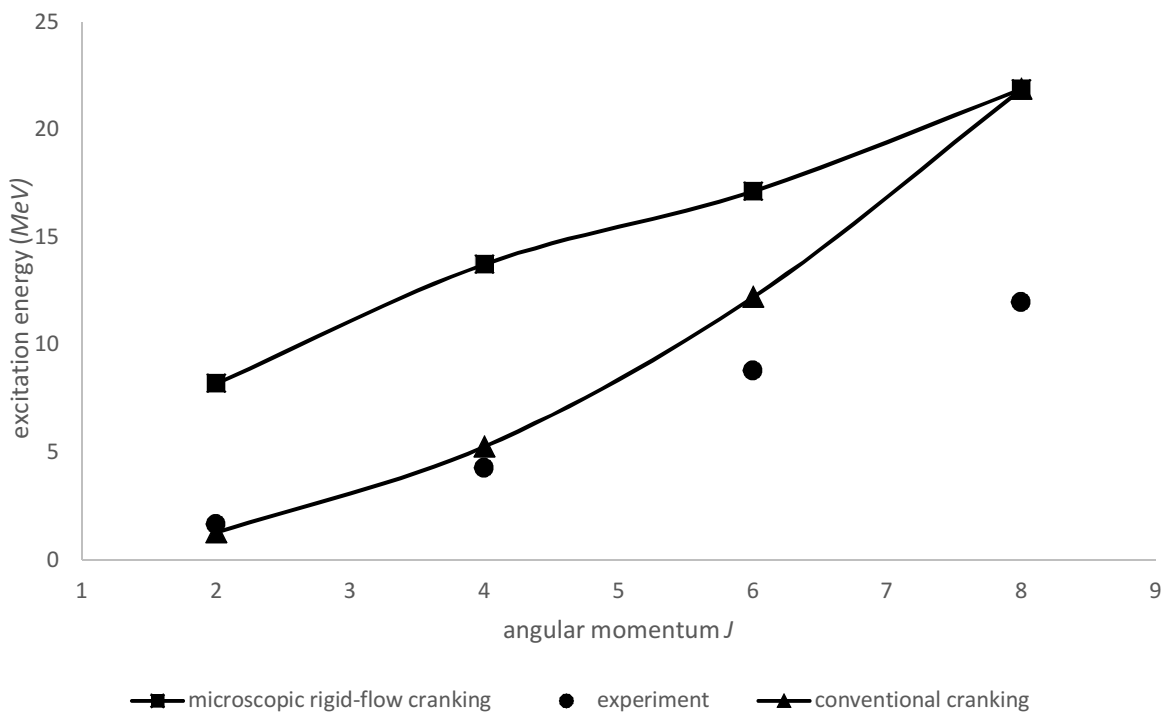


Fig 4: quadrupole moment versus  $J$  for self-consistency at all  $J$

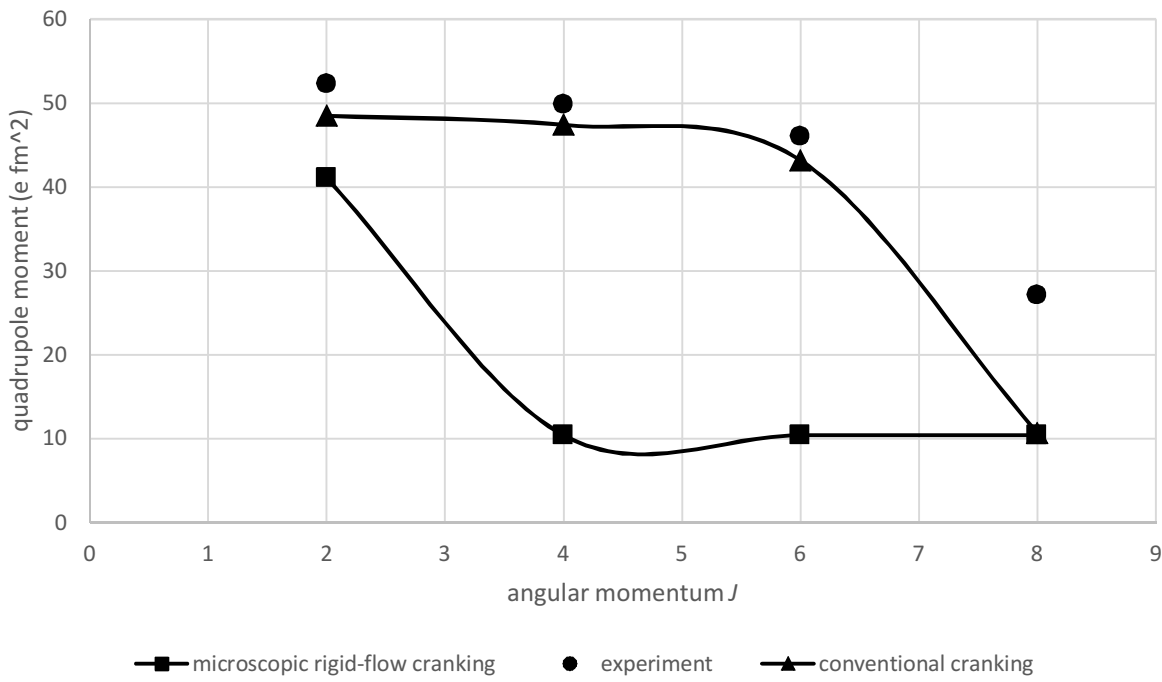
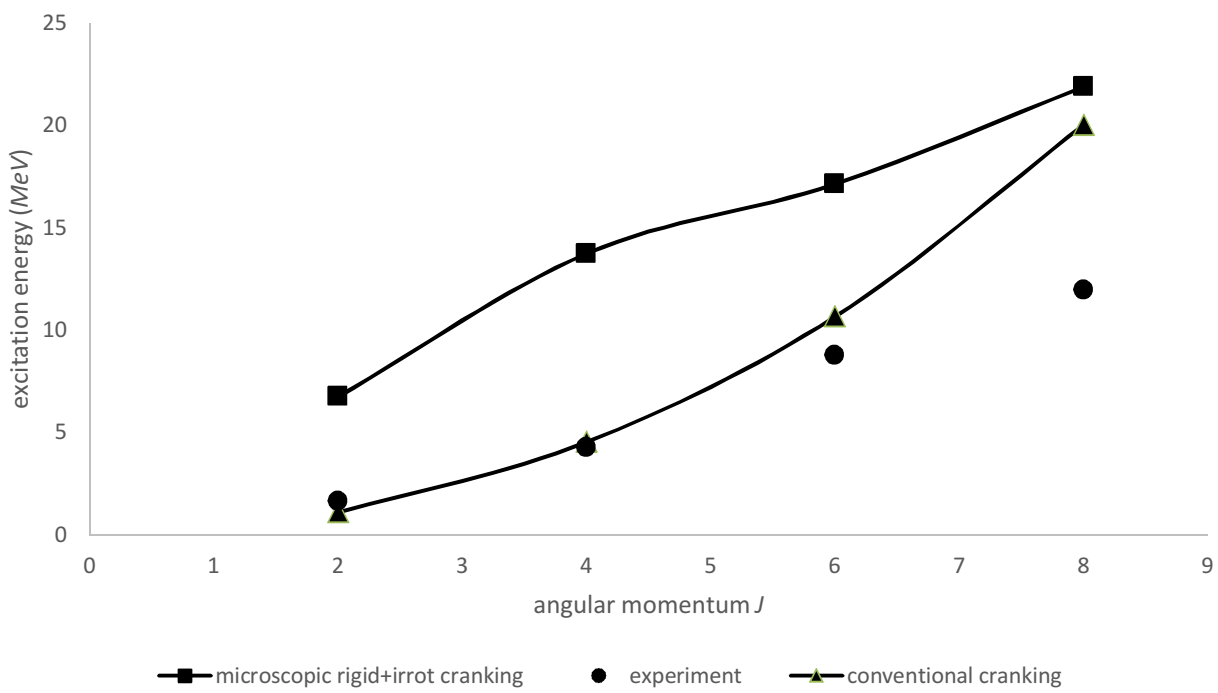


Fig 5: excitation energy versus  $J$  for selfconsistency at all  $J$



## 5. Correspondence between microscopic cranking and other collective rotational models

In this section, we reduce that the microscopic cranking model Eq. (43) or Eq. (48) to the equation of the conventional cranking model, nuclear particle-plus-rotor model, phenomenological and microscopic nuclear collective rotation-vibration models, and phenomenological classical collective rotation models.

### 5.1 Correspondence with conventional cranking model

The results of the calculation in Section 4.2 indicate that the microscopic cranking model predicts values of  $\omega_{rs}^o$  significantly higher than  $\omega_{cr}$  predicted by the conventional cranking model. This happens because we have determined  $\omega_{rs}^o$  using  $\hbar\gamma = \omega_{rs}^o \cdot M \cdot \mathcal{J}^o$  (Eq. (42)) and the constraint  $J = \gamma + l$  (Eq. (32)). On the other hand, the conventional cranking model uses the constraint  $J = l$ , and hence assumes implicitly that the angular momentum  $\hbar\gamma$  of the rotating frame is negligibly small. To match the microscopic and conventional cranking model equations, we must therefore assume that  $\gamma$  is negligibly small. Eq. (32) then becomes:

$$l = J - \gamma \approx J \quad (52)$$

Furthermore, the parameters in microscopic cranking model Eq. (43) or Eq. (48) are nearly independent of  $\lambda$ , i.e., the contribution from the term  $\lambda \cdot T$  in Eq. (43) is small, as noted in Section 3.2 in connection with Eq. (50). Therefore, we can drop the term involving  $\lambda$  in  $l$ . Eq. (52) then becomes identical to Eq. (5), and hence  $\omega_{rs}^o$  becomes identical to  $\omega_{cr}$ . It then follows that the microscopic cranking model energy  $E$  in Eq. (48) and the conventional cranking model energy  $E_{cr}$  in Eq. (37) become identical if the centrifugal energy in Eq. (48) is set equal to the Coriolis energy term in Eq. (37), i.e., if the following equation holds:

$$\frac{1}{2} \omega_{cr} \cdot M \cdot \left[ (1 + \lambda^2) \cdot \mathcal{J}_+^o - 2\lambda \cdot \mathcal{J}_-^o \right] = \langle \Phi_{cr} | L | \Phi_{cr} \rangle \equiv \hbar l \quad (53)$$

where we have set  $\omega_{rs}^o = \omega_{cr}$ . Solving Eq. (53) for  $\lambda$ , we obtain:

$$\lambda = \frac{\mathcal{J}_-^o}{\mathcal{J}_+^o} \left( 1 + \sqrt{1 + \frac{2\mathcal{J}_+^o \cdot \hbar l}{\omega_{cr} \cdot \mathcal{J}_-^{o2}} - \frac{\mathcal{J}_+^{o2}}{\mathcal{J}_-^{o2}}} \right) \quad (54)$$

where all the parameters on the right-hand-side of Eq. (54) are nearly independent of  $\lambda$ . We note that the factor  $\frac{\mathcal{J}_-^o}{\mathcal{J}_+^o}$  minimizes the energy  $E$  in Eq. (48) as stated in connection with Eq. (50).

Fig 6 shows the excitation energy predicted by the microscopic cranking model using  $\lambda$  in Eq. (54). Of course the excitation energies predicted by the microscopic and cranking models are identical by construction. However, Fig 7 shows that the value of  $\gamma$  predicted by the microscopic-model Eq. (42), i.e.,  $\hbar\gamma = \omega_{rs}^o \cdot M \cdot \mathcal{J}^o$ , is not small at all and in fact increases because both  $\mathcal{J}^o$  and  $\omega_{rs}^o$  increase with  $J$  as Fig 7 shows.

The inconsistency noted in the preceding paragraph between the value of  $\gamma$  assumed (as implied by the conventional cranking model, i.e., zero) and predicted (from  $\hbar\gamma = \omega_{rs}^o \cdot M \cdot \mathcal{J}^o$ ) by the microscopic model may be resolved by adding other flow regimes (such non-quadrupole rigid flow) to the rigid-irrotational flow regime in Eqs. (18) and (19) such that, in the prescription  $\hbar\gamma = \omega_{rs}^o \cdot M \cdot \mathcal{J}^o$ ,  $\mathcal{J}^o$  decreases as  $\gamma$  decreases but  $\omega_{rs}^o$  remains finite (which seems to be implied in the comparison between the conventional cranking and rotor models in [8], refer to Section 5.2 for more discussion). This approach will be considered in a future article.

Fig 6: excitation energy versus  $J$  - irrotational flow parameter chosen to match microscopic and conventional cranking model energies

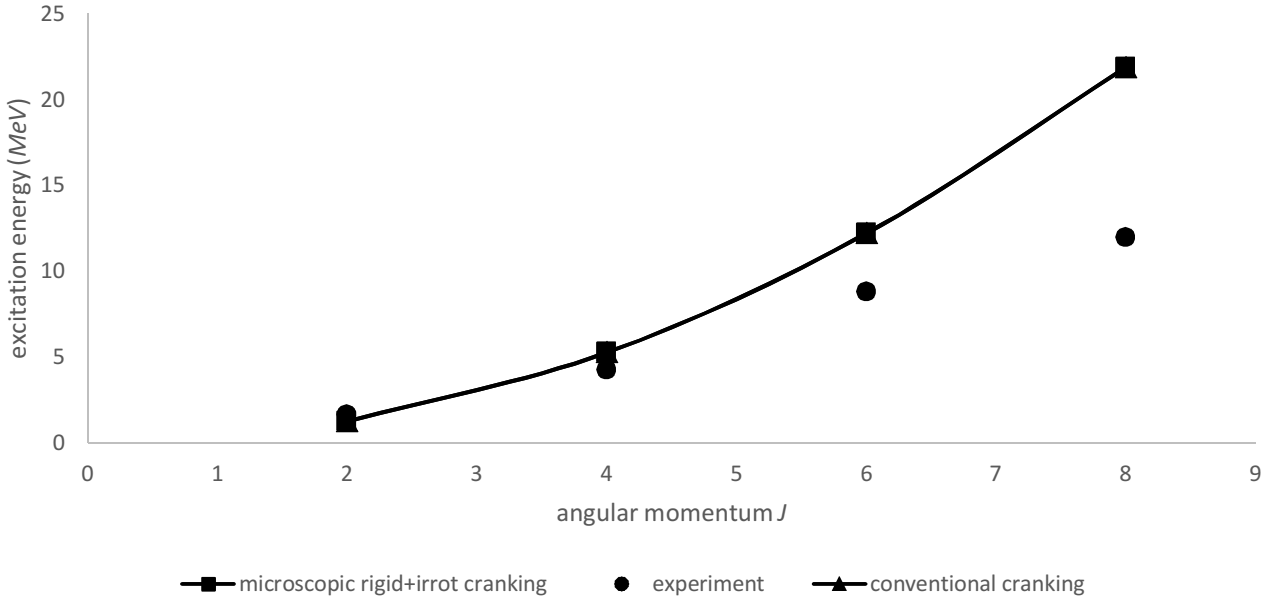
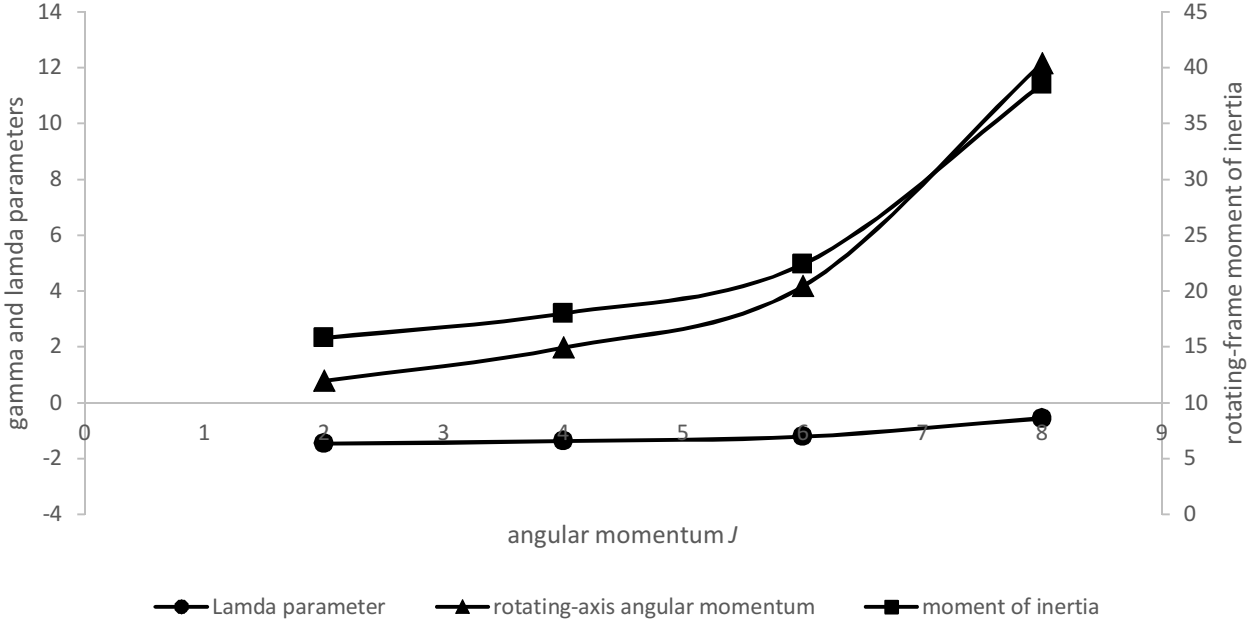


Fig 7: rotating-frame angular momentum and moment of inertia and irrotational-flow parameter versus  $J$



## 5.2 Correspondence with particle-plus-rotor model

As noted in Section 5.1, we can drop the small term  $\lambda \cdot T$  in Eq. (43) to obtain:

$$\left\{ H + \omega_{rs}^o \cdot L + \frac{\hbar^2 \gamma^2}{2M \mathcal{J}^{o2}} \left[ (1 + \lambda^2) \cdot \mathcal{J}_+^o - 2\lambda \cdot \mathcal{J}_-^o \right] \right\} \cdot \Phi = E \cdot \Phi \quad (55)$$

When  $\omega_{rs}^o$  is replaced by  $\frac{\hbar \gamma}{M \cdot \mathcal{J}^o}$  (Eq. (42)) and  $\gamma$  is replaced by  $J - l$  (Eq. (32)), Eq. (55)

becomes:

$$\left\{ H + \frac{\hbar(J-l)}{M \cdot \mathcal{J}^o} \cdot L + \frac{\hbar^2 (J-l)^2}{2M \mathcal{J}^{o2}} \left[ (1 + \lambda^2) \cdot \mathcal{J}_+^o - 2\lambda \cdot \mathcal{J}_-^o \right] \right\} \cdot \Phi = E \cdot \Phi \quad (56)$$

The Hamiltonian of the nuclear particle-plus-rotor model for rotation about a single axis is [4-7,12,28,39,57]:

$$H_{rp} \equiv H + \frac{\hbar(J - \hat{j})^2}{\mathcal{J}_{rp}} \quad (57)$$

where  $\hat{j}$  is the sum of the angular momentum operators of all the valence (out-of-core) nucleons and  $\mathcal{J}_{rp}$  is the core moment of inertia. The mean-field part of  $H_{rp}$  in Eq. (57) is:

$$H_{rp} \equiv H + \frac{2\hbar(J-j)}{\mathcal{J}_{rp}} \cdot (J - \hat{j}) = H - \frac{2\hbar(J-j)}{\mathcal{J}_{rp}} \cdot \hat{j} + \frac{2\hbar(J-j)J}{\mathcal{J}_{rp}} \quad (57)$$

where  $j$  is the mean of where  $\hat{j}$ . We may identify the second and the third terms on the right-hand-side of Eq. (57) with respectively the second and third terms on the left-hand-side of Eq. (56), keeping in mind that the angular momentum operator  $L$  includes the angular momenta of all the nucleons whereas  $\hat{j}$  includes only the valence (out of core) nucleons. This comparisons shows the correspondence between the microscopic cranking and rotor-plus-particle models.

The correspondence between the microscopic and conventional cranking models and between the microscopic cranking and particle-plus-rotor models establish a correspondence between the conventional cranking and particle-plus-rotor models. The latter correspondence elucidates the comparison between the rotor and conventional cranking models presented in [8]. We note that in the rotor model in [8], the only coupling between the rotational and intrinsic motion is through the assumed three moments of inertia, which are calculated using the conventional cranking model. We therefore, infer, from a comparison of Eq. (56) and the rotor model equation in [8], that the rotor model assumes the condition  $L \cdot \Phi = 0$ . However, in [8] a quantum analogue of the conventional cranking model was surmised in the following form (for rotation along a single axis):

$$H_{rp} \equiv H - \frac{\hbar J \cdot L}{\mathcal{J}_{rp}} \quad (58)$$

Eq. (58) resembles the coupled  $J \cdot L$  term in the first term on the left-hand-side of Eq. (56).

### 5.3 Correspondence with phenomenological and microscopic rotational models

When we impose zero angular momentum constraint (i.e.,  $L \cdot \Phi = 0$ ) on the intrinsic wavefunction  $\Phi$  so that  $\gamma = J$ , and set  $\lambda = 0$ , Eq. (55) becomes:

$$\left( H + \frac{\hbar^2 J^2}{2M\mathcal{J}_+^o} \right) \cdot \Phi = E \cdot \Phi \quad (59)$$

Eq. (59) is identical to the rotational part in the equations of the microscopic [38,55,56] and phenomenological [3] collective rotation-vibration models for rotation about a single axis.

## 5.4 Correspondence with phenomenological classical collective rotational models

When we impose the constraints  $L \cdot \Phi = 0$  and  $H \cdot \Phi = 0$  (i.e., no intrinsic motion) so that  $\gamma = J$ , Eq. (55) becomes:

$$\frac{\hbar^2 J^2}{2M\mathcal{J}^o} \left[ (1 + \lambda^2) \cdot \mathcal{J}_+^o - 2\lambda \cdot \mathcal{J}_-^o \right] \cdot \Phi = E \cdot \Phi \quad (60)$$

Eq. (60) may be considered to be a quantum version of the classical collective two-fluid rotational models [40,41,42,45] with only one (namely  $\lambda$ ) free parameter (the other parameter is determined in Eq. (20) by the commutation relation  $[\theta, L] = i\hbar$ ).

## 6. Concluding remarks

The conventional cranking model is often used to study rotational properties of nuclei. In view of its importance in nuclear structure studies and its phenomenological and semi-classical basis, it is desirable to have a better understanding of the assumptions and approximations that underlie the model derivation. In the hope of achieving this objective, we have attempted, in this article, to derive the model simply and from first principles by transforming the nuclear Schrodinger equation (instead of the Hamiltonian) to a rotating reference frame using a particle-plus-rotor rotation-intrinsic product wavefunction and imposing no constraints on either the wavefunction or the particle coordinates. The rotation of the reference frame is chosen to be generated by the motions of the nucleons instead of being imposed externally, unlike that in the conventional cranking model. As a consequence, the microscopic model Schrodinger equation is time reversal invariant, unlike the conventional cranking model. In this article, the rotation of the reference frame is chosen to be determined by a combination of rigid and irrotational flows of the nucleons.

The resulting transformed Schrodinger equation resembles that of the conventional cranking model in a space-fixed frame. However, the angular velocity in the microscopic model is not a constant parameter but is a dynamical variable determined by angular momentum of the rotating frame and an associated kinematic moment of inertia. This moment is determined by the nature of the aforementioned rigid-irrotational flow combination. The angular momentum of the rotating frame is determined by requiring the expectation of the total angular momentum to have rotational-band member state angular momentum. This expectation is a sum of the angular momenta of the rotating frame and intrinsic system. It turns out that the rotations of the intrinsic system and rotating frame are in opposite directions. Furthermore, the transformed Schrodinger equation has, in addition to the Coriolis energy term, a rigid-flow centrifugal kinetic energy term that is absent from the conventional cranking model Schrodinger equation.

In this article, we suppress the fluctuations in the angular velocity and their coupling to the intrinsic motion by replacing the kinematic moments of inertia by their expectation values in each intrinsic-system state. We do so because we are interested in comparing the model with the conventional cranking model, which ignores such fluctuations. Furthermore, a preliminary

calculation seems to show that the impact of the fluctuations is relatively small. The resulting Schrodinger equation is then solved for a deformed harmonic oscillator mean-field potential. The oscillator frequencies are determined self-consistently from numerical minimization of the energy subject to a constant nuclear volume condition.

Using the microscopic cranking model, we calculate the excitation energy and quadrupole moment for the ground-state rotational band of the nucleus  $^{20}_{10}Ne$ . The results for rigid flow case show that the model predictions have trends similar to those of the conventional cranking model except that the intrinsic angular momentum has a significantly higher maximum absolute value (in order to reduce the high rotating-frame angular momentum to the rotational-band member state angular momentum). The predicted excitation energy is significantly higher than the measured one. The predicted quadrupole moment is smaller than that measured. Adding an irrotational flow component to the rigid-flow rotation of the rotating frame is found to somewhat improve the agreement with the results of the conventional cranking model and measurement at  $J = 2$ . However, at higher  $J$  values the irrotational flow component has little effect because the rotating-frame moment of inertia is reduced to the rigid-flow moment.

It is shown that the microscopic cranking model equation becomes identical to those of the conventional cranking model for a particular choice of the combination of the rigid and irrotational flows and when the rotating-frame angular momentum is assumed to be negligibly small. These results seem to indicate that the conventional cranking model implicitly assumes that the rotating frame has negligibly small angular momentum and that the frame rotation is to some extent governed by combined rigid and irrotational flows of the nucleons.

We have also shown that the microscopic cranking model equation can be reduced to that of the nuclear particle-plus-rotor model, microscopic and phenomenological collective rotation-vibration models, and phenomenological classical collective rotational models.

In future studies, we will attempt to strengthen the correspondence between the microscopic and conventional cranking models by using additional flow regimes such a non-quadrupole rigid flow. We will also generalize the microscopic cranking model to three dimensions.

## References

- [1] D. R. Inglis, Phys. Rev. 103 (1956) 1786.
- [2] D.J. Thouless and J.G. Valatin, Nucl. Phys. 31 (1962) 211.
- [3] J.M. Eisenberg and W. Greiner, Nuclear Theory (North-Holland, Amsterdam, 1970).
- [4] D.J. Rowe, Nuclear Collective Motion (Mathuen and Co. Ltd., London, 1970).
- [5] R.A. Sorensen, Rev. Mod. Phys. 45 (1973) 353.

- [6] A. deShalit and H. Feshbach, *Theoretical Nuclear Physics*, Vol. 1 (John Wiley & Sons, Inc., N.Y., 1974).
- [7] A. Bohr and B.R. Mottelson, *Nuclear Structure*, Vol. II (Benjamin, N.Y., 1975).
- [8] G. Ripka, J.P. Blaizot, and N. Kassis, in *Heavy-Ion, High-Spin States and Nuclear Structure*, Vol. 1, Trieste Int. Seminar on Nuclear Physics, September 17-December 21, 1973 (IAEA, Vienna, 1975).
- [9] R.M. Lieder and H. Ryde. in *Advances in nuclear physics*. Vol. 10, edited by M. Baranger and E. Vogt. Plenum Press, New York. 1978.
- [10] R. Bengtsson and S. Frauendorf, *Nucl. Phys. A* 314, (1979) 27.
- [11] W.D. Heiss and R.G. Nazmitdinov, *Phys. Letts. B* 397 (1997) 1.
- [12] P. Ring and P. Schuck, *The Nuclear Many-Body Problem* (Springer-Verlag, N.Y., 1980).
- [13] A.L. Goodman, G.S. Goldhaber, A. Klein, and R.A. Sorensen, *Nucl. Phys. A* 347 (1980).
- [14] A. Faessler, in *Proc of Conf. on High Angular Momentum Properties of Nuclei*, Proc. Oak Ridge, Tennessee, November 2-4, 1982, Vol. 4, edited by N.R. Johnson, Hardwood Academic Publishers N.Y. 1982.
- [15] F.S. Stephens. in *Frontiers in nuclear dynamics*. edited by R.A. Broglia and C.H. Daso, Plenum Press, New York. 1985.
- [16] S.G. Nilsson and I. Ragnarsson, *Shapes and shells in nuclear structure* (Cambridge University Press, Cambridge, UK. 1995).
- [17] T. Tanaka, F. Sakata, T. Marumori, and K. Iwasawa. *Phys. Rev. C* 56 (1997) 180.
- [18] A. Klein, *Phys. Rev. C* 63 (2000) 014316.
- [19] S. Frauendorf, *Rev. Mod. Phys.* 73 (2001) 463.
- [20] W.D. Heiss and R.G. Nazmitdinov, *Phys. Rev. C* 65 (2002) 054304.
- [21] R.G. Nazmitdinov, D. Almehed, F. Donau, *Phys. Rev. C* 65 (2002) 041307.
- [22] M. Matsuzaki, Y.R. Shimizu, and K. Matsuyanagi, *Phys. Rev. C* 65 (2004) 034325.
- [23] M.A. Deleplanque, S. Frauendorf, V.V. Pashkevich, S.Y. Chu, and A. Unzhakova, *Phys. Rev. C* 69 (2004) 044309.
- [24] A.V. Afanasjev, arXiv [nucl-th] 1510.08400, October 28, 2015.

[25] A.G. Magner, D.V. Gorpichenko, and J. Bartel, arXiv [nucl-th] 1604.06866, April 23, 2016.

[26] T. Nakatsukasa, K. Matsuyanagi, M. Matsuzaki, Y.R. Shimizu, arXiv [nucl-th] 1605.01876, May 06, 2016.

[27] A.F. Stamp, Nucl. Phys. 164 (1971) 81.

[28] A.B. Bohr and B.R. Mottelson, Physica Scripta 22 (1980) 461.

[29] R.E. Peierls and J. Yoccoz, Proc. Phys. Soc. 70 (1957) 381.

[30] A. Bohr and B. Mottelson, Forh. Norske Vidensk. Selsk. 31 (1958) No. 12.

[31] F. Villars and N. Schmeing-Rogerson, Ann. Phys. 63 (1971) 443.

[32] F. Villars and G. Cooper, Ann. Phys. (N.Y.) 56 (1970) 224.

[33] A. Bohr, Kgl. Dan. Mat. Fys. Medd. 26 (1952) 14.

[34] A.S. Davydov and G. F. Filippov, Nucl. Phys. 8 (1958) 237.

[35] A. Faessler and W. Greiner, Z. Physik 180 (1962) 425.

[36] P. Gulshani, arXiv [nucl-th] 1502.07590, May 12, 2015.

[37] P. Gulshani, Can. J. Phys. 94 (2016) 79.

[38] P. Gulshani, arXiv [nucl-th] 1602.01324, July 15, 2016.

[39] B.J. Verhaar, A.M. Schulte, and J. de Kam, Z. Physik A 277 (1976) 261.

[40] R.Y. Cusson, Nucl. Phys. A 114 (1968) 289.

[41] V.R. Prakash, B.M. Bahal, and V.K. Deshpanda, Can. J. Phys. 50 (1972) 2957.

[42] V.R. Prakash and V.K. Deshpanda, Can. J. Phys. 51 (1973) 1752.

[43] P. Gulshani and D.J. Rowe, Can. J. Phys. 54 (1976) 970.

[44] B. Buck, L.C. Biedenharn, and R.Y. Cusson, Nucl. Phys. A 317 (1979) 205.

[45] M.A. Habeeb, R.F. Bishop, J.M. Irvine, and M.R. Strayer, J. Phys. G: Nucl. Phys. 4 (1978) 857.

[46] P. Gulshani, Nucl. Phys. A 832 (2010) 18.

[47] T. Gustafson, Dan. Mat. Fys. Medd. 30 (1955) No. 5.

[48] G. Rosensteel, Phys. Rev. C 46 (1992) 1818.

- [49] I.N. Mikhailov, P. Quentin, and D. Samson, Nucl. Phys. A 627 (1997) 259.
- [50] J.G. Valatin, Proc. Roy. Soc. (London) 238 (1956) 132.
- [51] V.G. Zelevinskii, Sov. J. Nucl. Phys. 22 (1976) 565.
- [52] A.P. Stamp, Z. Physik A 284 (1878) 312.
- [53] T. Troudet and R. Arvieu, Ann. Phys. 134 (1981) 1.
- [54] P. Gulshani and A. B. Volkov, J. Phys. G: Nucl. Phys. 6 (1980) 1335.
- [55] P. Gulshani, Can. J. Phys. 94 (2016) 79.
- [56] P. Gulshani, arXiv [nucl-th] 1502.07590, May 12, 2015.
- [57] J. Almberger, I. Hamamoto, and G. Leander, Nucl. Phys. A333 (1980) 184.